Applied Physics Reviews REVIEW pubs.aip.org/aip/are

Quantum dot in perovskite hybrids for photovoltaics: Progress and perspective

Cite as: Appl. Phys. Rev. **11**, 041329 (2024); doi: 10.1063/5.0218208
Submitted: 9 May 2024 · Accepted: 21 October 2024 ·
Published Online: 5 December 2024

View Online Export Citation CrossMark

Hyung Ryul You,[1] Han Na Yu,[1] Eon Ji Lee,[1] Hyeon Soo Ma,[1] Younghoon Kim,[2,a)] and Jongmin Choi[1,a)]

AFFILIATIONS

[1]Department of Energy Science and Engineering, Daegu Gyeongbuk Institute of Science and Technology (DGIST), Daegu 42988, Republic of Korea
[2]Department of Chemistry, Kookmin University, Seoul 02707, Republic of Korea

Note: This paper is part of the APR Special Topic on Quantum Metamaterials.
[a)]**Authors to whom correspondence should be addressed:** younghoon.kim@kookmin.ac.kr and whdals1062@dgist.ac.kr

ABSTRACT

Colloidal quantum dots (CQDs) are receiving great attention as promising nanomaterials for optoelectronic applications due to their unique electronic properties and straightforward processability. Despite extensive global research and significant progress in the surface chemistry and device architecture of CQDs, meeting the future demands for stability and device performance continues to be a challenge. Recently, innovative matrix engineering strategies that introduce a dot-in-perovskite structure have been recognized as breakthroughs in overcoming these challenges. This review chronicles the advancements of CQD-perovskite hybrids and discusses future perspectives, particularly regarding lead sulfide (PbS) CQDs for infrared photovoltaic applications.

TABLE OF CONTENTS

I. INTRODUCTION

Developing renewable energy systems is an essential task for humanity in the 21st century. In solar energy, despite the commercial success of silicon (Si)-based photovoltaics, their expensive processing and limited absorption spectrum necessitate the exploration of advanced optoelectronic materials.[1–3] Colloidal quantum dots (CQDs) are promising candidates for optoelectronic applications, such as photovoltaics and photodetectors, due to their unique optoelectronic properties and ease of processing.[4–13] In particular, CQD-based photovoltaic devices are well-suited for small-scale systems like wearable applications. Additionally, they have the potential to be scaled up for larger energy conversion applications, such as rooftop installations, by being combined with other materials in tandem devices. Through the quantum confinement effect, the electronic structures of these materials can be precisely tuned by altering the size or shape of the crystals, without changing their chemical composition. Moreover, the quantized energy levels within band structure of CQDs delay the release of phonons, which eventually enables the formation of two or more excitons from a single photon, a phenomenon known as multiple exciton generation (MEG) that could be a breakthrough in maximizing photovoltaic performance.[5,6] Among various CQDs, lead sulfide (PbS) CQDs possess desirable properties for optoelectronics.[14,15] The PbS crystal exhibits a high absorption coefficient due to its direct bandgap and the high density of states (DOS) in the conduction band, which is composed of the Pb 6p orbital, enabling strong photon absorption. More importantly, the combination of a bulk bandgap of 0.41 eV and a large exciton in Bohr radius of 20 nm allows it to have infrared (IR) capabilities with an easily tunable absorption range. With these advantages, PbS CQDs have been intensively studied in terms of surface chemistry and device architecture, leading to remarkable improvements of photovoltaic performance in recent decades.[16–26]

The surface passivation strategies based on organic–inorganic ligands, especially the molecular lead halide (PbX_2, X = I, Br) ligands, provided a foundation to achieve recent air stable and efficient CQD devices.[16] These advances enabled CQD photovoltaics to obtain over 90% of initial power conversion efficiency (PCE) value after few months in ambient conditions,[18,20,21,23] which cannot be achieved in prior studies that the encapsulation of CQD device was indispensable due to the poor ambient stability.[16] However, despite these advances, the stability and device performance of CQDs seems still lacking to reaching the commercialization level, and these are mainly attributed to inhomogeneous electronic energy landscape and trap levels from physical aggregation of CQDs accompanied by surface degradation such as ligand losses, especially accelerated in thermal and humid conditions.[16,21,26] In 2015, a promising strategy for realizing quantum dot-in-perovskite hybrids was reported, marking a breakthrough in enhancing device performance and stability in the field of CQDs.[27] The perovskites, with a chemical formula of ABX_3 (where A, B, and X represent a monovalent cation, a divalent cation, and a monovalent anion, respectively), have gained attention as optoelectronic materials in recent decades due to their advantageous properties, such as long diffusion lengths and high absorption coefficients. The first-principle density functional theory (DFT) calculations of this study showed that methylammonium lead iodide perovskites ($MAPbI_3$) can epitaxially grow on PbS CQD surfaces. The heteroepitaxial interface between these two materials enables the realization of a dot-in-perovskite structure, wherein the PbS CQDs are embedded within a $MAPbI_3$ matrix with atomic-level coherence. Initially, this study aimed to create an electrical-optical synergy effect between the two materials. However, the dot-in-perovskite concept has proven potentially transformative, leading to new strengths in various applications.[28–41] Since this initial report, the hybrid structures of CQD-perovskites with various compositions have been explored for their potential in optoelectronic applications. A notable advantage of these hybrids is the lattice anchoring effect, which extends beyond merely passivating the surfaces of CQDs. In 2019, it was discovered that the $CsPbX_3$ (X = I, Br) perovskite matrix physically protects PbS CQDs from aggregating, while the lattice anchoring of the CQD maintains the desirable cubic phase of the perovskite matrix, counteracting the tendency for unstable phase transitions.[34] These findings suggest that effective hybridization of CQD and perovskite may address challenges that have persisted over the past decades. From this perspective, this article provides a concise review of quantum dot-in-perovskite hybrids, focusing on PbS CQD and lead halide perovskites, categorized primarily by perovskite cation composition. After that, we will discuss the future research directions for this hybrid to further enhance its potential.

II. EMERGING DOT-IN-PEROVSKITE STRATEGIES

A. MA-cation-based perovskite matrix for photovoltaics

Lead halide perovskites are promising materials for next-generation solar cells due to their excellent optical, electrical features.[42–47] Meanwhile, PbS CQDs have a highly tunable absorption range that includes near to short infrared (NIR-SWIR) harvesting capabilities, which lead halide perovskites have failed to access.[14,15,19–23] Initially, the dot-in-perovskite hybrid structure of PbS CQD and methylammonium lead iodide perovskite ($MAPbI_3$) was reported by Ning *et al.* to combine the strengths of both materials.[27] The DFT results of this study revealed that the PbS crystal and the $MAPbI_3$ perovskite form with less than 5% lattice mismatch and an interfacial energy lower than 10 meV/Å^2. This enables the heteroepitaxial growth of $MAPbI_3$ perovskite on PbS CQD surfaces. Based on this concept, they realized the quantum dot-in-perovskite matrix system by epitaxially growing the $MAPbI_3$ perovskite in CQD films through soaking in an MA-dissolved isopropyl alcohol (IPA) solution [Fig. 1(a)]. The heteroepitaxial characteristic of the dot-in-perovskite film forms defect-free interfaces, resulting in enhanced photoluminescence quantum efficiency (PLQE) of 9.3%, compared to 1% for the bare CQD film. Experimentally, the coexistence of CQD and perovskite was verified using x-ray photoelectron spectroscopy (XPS), Rutherford backscattering spectroscopy (RBS), and high-resolution transmission electron microscopy (HRTEM). After this finding, using the PbS-$MAPbI_3$ dot-in-perovskite, Yang *et al.* demonstrated CQD photovoltaics with an 8.95% PCE in the same year [Fig. 1(b)].[28] This research team also suggested using a perovskite precursor-dissolved CQD ink for a single-step process, differing from the precursor-soaking method used previously.

This dot-in-perovskite strategy is not limited to CQD-based devices. In the field of perovskites, the challenges lie in controlling film morphologies, crystallinity, pinholes, and achieving high surface coverage to avoid low shunting paths.[43,48] To address these issues, in 2016, Li *et al.* reported a method involving doping a small amount (0.5–1.5 wt. %) of PbS CQDs into perovskite precursor inks.[29] The MAI-treated PbS CQDs can be dispersed homogeneously in the perovskite inks. This method enabled heterogeneous nucleation of perovskite on CQD surfaces, resulting in enhanced crystallinity of the perovskite film [Fig. 1(c)]. Specifically, with a doping amount of 1 wt. %, this strategy resulted in a relative ∼25% PCE enhancement of perovskite photovoltaics (PCE of 17.4%) compared to the reference device (PCE of 14.11%). Following this research, Han *et al.* also reported an increased crystal size of $MAPbI_3$ perovskite through embedding the PbS CQDs strategy, resulting in a PCE of 18.6%, compared to that of bare $MAPbI_3$ perovskite photovoltaics (16.3%).[40] The increase in power conversion efficiency (PCE) was primarily attributed to the rise in short-circuit current density (J_{SC}), which resulted from the increased crystal size of $MAPbI_3$ perovskite.

B. Inorganic cation-based perovskite matrix for photovoltaics

Realizing dot-in-perovskite systems requires sophisticated lattice matching and low interfacial energy between CQDs and perovskites. Although dot-in-perovskite hybrids between PbS CQD and organic MA cation-based lead halide perovskite have been constructed in previous studies, a lattice mismatch of around 5% still exists.[27] Therefore, achieving further improvement in this area necessitates the exploration of new material compositions. In 2017, Jung *et al.* reported that cesium lead bromide perovskite ($CsPbBr_3$) exhibits a lattice match of less than 1% with PbS CQD, facilitating the formation of a higher-quality epitaxial interface [Fig. 2(a)].[32] In the following year, Zhang *et al.* reported a CQD solar cell incorporating a $CsPbI_3$-PbS structure.[33] Compared to conventional organic MA cation-based lead halide perovskites (with the device reported in 2015 exhibiting a PCE of 8.95%, an open-circuit voltage V_{OC} of 0.61 V, a short-circuit current density J_{SC} of 21.8 mA/cm^2, and a fill factor FF of 67.9%), the $CsPbI_3$-based PbS-perovskite

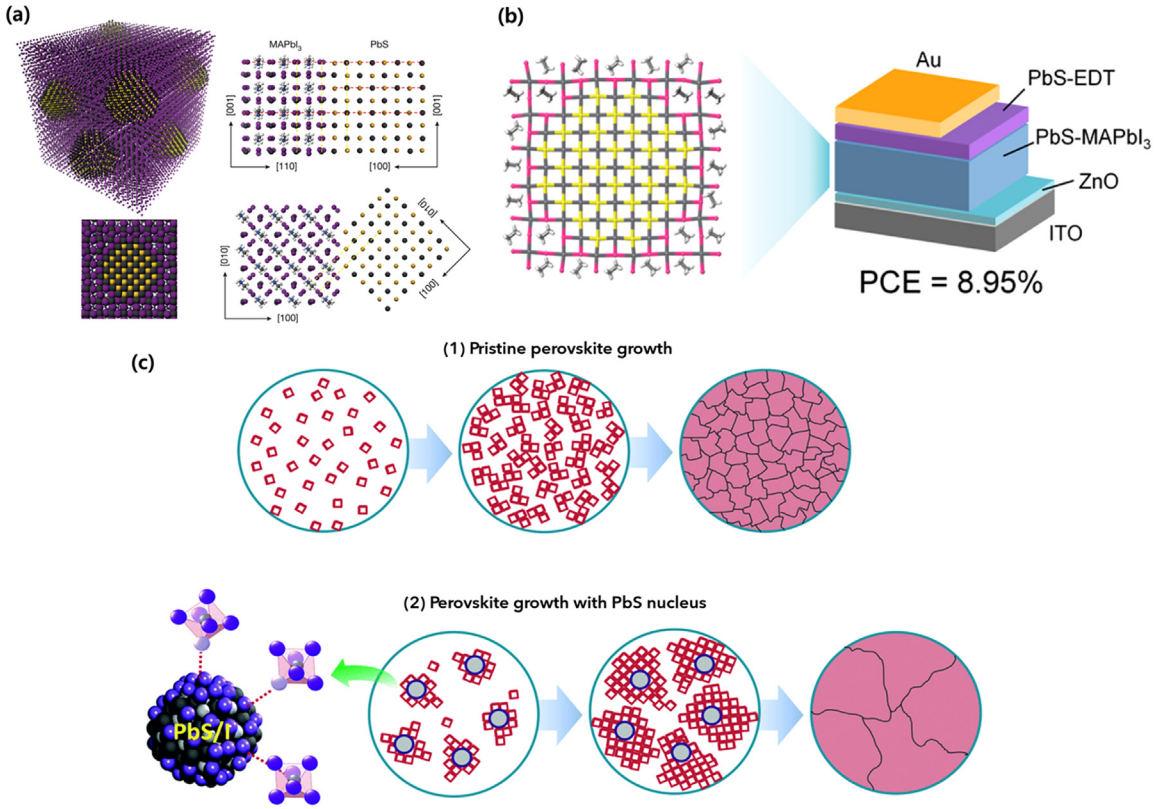

FIG. 1. (a) An atomistic model of CQDs in a perovskite matrix and modeling of the PbS and $MAPbI_3$ crystal structures and their interface, showing that the perovskite matches well with the PbS crystal (the red dashes indicate the unit cell size; the yellow dashes are guides to the eye for matching planes). Reproduced with permission from Nature **523**, 324–328 (2015). Copyright 2015 Springer Nature.[27] (b) The schematic of the CQD photovoltaic featuring the PbS-$MAPbI_3$ dot-in-perovskite structure. Reproduced with permission from Nano Lett. **15**, 7539–7543 (2015). Copyright 2015 American Chemical Society.[28] (c) Proposed nucleation and growth routes of perovskite crystal thin films with and without PbS CQDs; this includes the assisted formation of lead halide octahedrons in the vicinity of PbS CQDs. Reproduced with permission from Energy Environ. Sci. **9**, 1282–1289 (2016). Copyright 2016 Royal Society of Chemistry.[29]

structure demonstrated enhanced photovoltaic parameters, achieving a PCE of 10.5%, a V_{OC} of 0.64 V, a J_{SC} of 24.5 mA/cm^2, and an FF of 67%, along with a significant reduction in hysteresis.[28,33] This result implies that superior lattice matching is essential for achieving higher device performance. To further enhance lattice matching, Liu *et al.* adjusted the halide anion composition of Cs-cation-based perovskites ($CsPbX_3$, X=Br, I) [Fig. 2(b)], creating a dot-in-perovskite structure with nearly 0% lattice mismatch. In 2019, they reported a PCE of 12.6% for the CQD photovoltaic, noting that PbS-$CsPbX_3$ (X=Br, I) hybrids exhibited a lattice mismatch of less than 0.2%, with a Br to I ratio of 2:1 [Fig. 2(c)].[34] To identify the correlation between lattice matching and the surface defect passivation effect, PLQE analysis was conducted. The dot-in-perovskite film with nearly 0% lattice mismatch showed a PLQE of approximately 30%, whereas the other composition, with a lattice mismatch of over 0.5%, exhibited a PLQE of under 15%. These results indicate that perfect lattice matching plays an important role in forming defect-free interfaces in CQD-perovskite hybrid films.

A notable effect of the dot-in-perovskite hybrid is the lattice-anchoring effect, which significantly improves the thermal stability of both perovskites and CQDs. Despite Cs-based lead halide perovskites being stable in the α-phase (cubic) $CsPbX_3$ (X=Br, I) in the mixed halide system, they become unstable due to phase separation caused by ion migration during heat treatment in air.[49,50] However, it was found that the phase transformation of perovskites from α to δ-phase is suppressed by the lattice anchoring effect when they are epitaxially grown on CQDs with perfect lattice matching. They studied the effect of CQD concentration on the thermal stability of the perovskite matrix. Additionally, they investigated the relationship between the composition of the perovskite and the concentration of CQDs, as different perovskite compositions induce varying levels of lattice strain, requiring distinct stabilization strategies. When the lattice-matched condition is achieved with a Br to I ratio of 2:1 ($CsPbBr_2I$), the absorbance intensity loss of the perovskite under 200 °C in air decreased linearly with increasing CQD volume percentage, demonstrating that the stability of the perovskite matrix is proportional to CQD concentration. Conversely, when the Br content is reduced (breaking the perfect lattice matching), the stability of the perovskite exhibited a V-shaped trend at lower CQD fractions [Fig. 2(d)]. This behavior is attributed to the low CQD

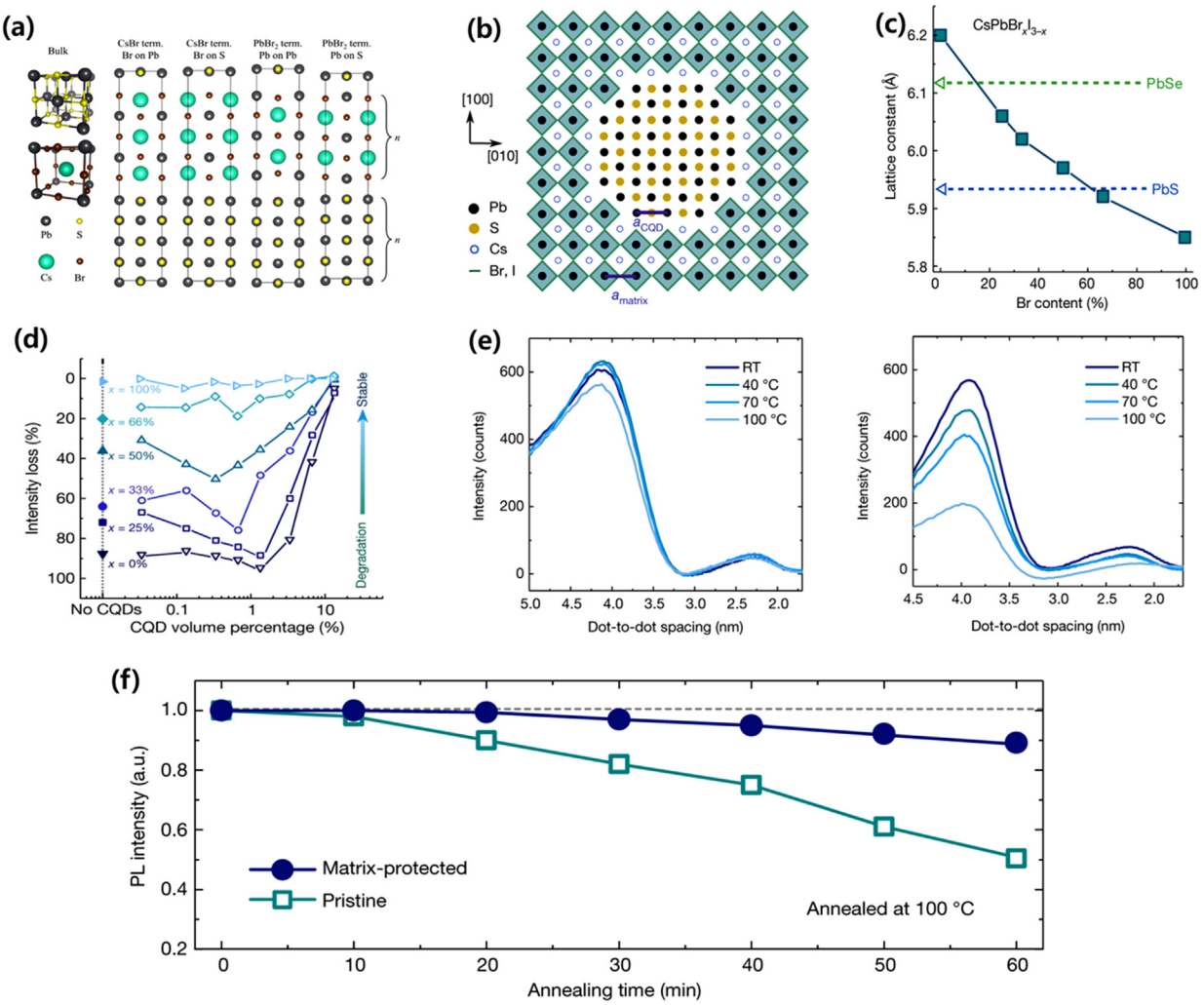

FIG. 2. (a) Atomic structures of PbS and $CsPbBr_3$ bulks along with four different interface models featuring various contact geometries. "CsBr" or "$PbBr_2$" refers to the terminations of the $CsPbBr_3$ (100) surface in contact with the PbS (100) surface. Reproduced with permission from J. Phys. Chem. C. **121**, 27351–27356 (2017). Copyright 2017 American Chemical Society.[31] The atoms of Pb, S, Cs, and Br are represented as black, yellow, green, and brown spheres, respectively. (b) Schematic representation of lattice-anchored $CsPbX_3$ (X=Br, I) perovskite on PbS CQDs. Reproduced with permission from Nature **570**, 96–100 (2019). Copyright 2019 Springer Nature.[34] (c) The lattice constant of PbS CQDs and $CsPbX_3$ perovskites as it varies with bromide content. Reproduced with permission from Nature **570**, 96–100 (2019). Copyright 2019 Springer Nature.[34] (d) The intensity loss in absorbance of perovskite film after 5 h of annealing in air (x is the content of Br). Reproduced with permission from Nature **570**, 96–100 (2019). Copyright 2019 Springer Nature.[34] (e) Changes in dot-to-dot spacing (uniformity) among CQDs at various annealing temperatures for matrix-protected (left) and bare (right) CQD films. Reproduced with permission from Nature **570**, 96–100 (2019). Copyright 2019 Springer Nature[34] and (f) Changes in photoluminescence (PL) intensity of matrix-protected (circle) and bare (square) CQD films following the annealing time at 100 °C. Reproduced with permission from Nature **570**, 96–100 (2019). Copyright 2019 Springer Nature.[34]

loading inducing significant interfacial strain, leading to the generation of atomic dislocations. Consequently, a higher CQD loading (over 13 vol. %) is necessary in lattice-mismatched systems to enhance the stability of the perovskite by inducing the lattice anchoring effect. As for CQDs, stability issues arise due to oxidation and aggregation, even at temperatures below 50 °C.[51,52] However, when embedded in a perovskite matrix, CQDs exhibit enhanced thermal stability thanks to the lattice-anchored perovskite matrix. To assess the stability of CQDs in perovskite at high temperatures (100 °C), GISAXS analysis was conducted [Fig. 2(e)]. The packing density of the bare CQD film began to degrade at 40 °C, whereas the matrix-protected CQD film remained stable. Additionally, in the PL analysis, the matrix-protected CQDs maintained 90% of their PL intensity after 1 hour of annealing at 100 °C, while the intensity of the bare CQD film decreased to less than 50% of its initial value [Fig. 2(f)]. These findings suggest that dot-in-perovskite hybrids could represent a breakthrough in addressing thermal stability issues in both CQDs and perovskite materials.

C. FA-cation-based perovskite matrix for photovoltaics

In recent composition engineering efforts in perovskite, it has been reported that the formamidinium (FA) cation in lead halide perovskite provides a narrower bandgap and higher thermal stability compared to MA or Cs cation-based perovskites.[47,53,54] Additionally, the lattice constants of $FAPbBr_3$ and $FAPbI_3$ perovskites (5.99 and 6.36 Å, respectively) are suitable for forming an epitaxial interface with PbS crystal.[37] Taking advantage of these benefits, recent dot-in-perovskite strategies have also started to incorporate $FAPbX_3$ (X = I, Br) perovskites.[36–38] Considering that perovskite typically exhibits a larger bandgap than PbS CQDs, it is probable that the electronic band structure in dot-in-perovskite systems is type-I. This suggests that using perovskites with narrower band gaps could decrease the dot-to-dot barrier for carrier tunneling. In 2020, Albaladejo-Siguan *et al.* reported that a CQD photovoltaic device achieved a PCE of 11.3% by incorporating FA-based triple-cation perovskite $[Cs_{0.05}(MA_{0.17}FA_{0.83})_{0.95}PbX_3$ (X= Br, I)] ligands.[36] Compared to PbS-$MAPbI_3$ and PbS-PbI_2 CQD photovoltaics, the triple-cation device exhibited lower charge recombination characteristics, resulting in a thicker optimized CQD film for the photovoltaics. Although the accurate origin is not identified in that study, they hypothesized that this is due to the relatively low energy barriers (0.3 eV for electrons and 0.2 eV for holes) of type-I band alignment between triple-cation perovskite and PbS CQDs does not impede charge extraction.

In the same year, Bin *et al.* reported achieving a PCE of 13.8% in CQD photovoltaics (compared to 11.8% PCE of conventional CQD device) by introducing a dot-in-perovskite structure based on $FAPbBr_3$.[37] In this study, they proposed an experimental process aimed at enhancing carrier transport efficiency within the dot-in-perovskite film by reducing the thickness of the perovskite matrix. Instead of using the conventional method of mixing perovskite with CQD ink, they soaked the perovskite precursor-dissolved acetonitrile (ACN) solution onto the CQD film [Fig. 3(a)]. This approach enabled the fabrication of an ultra-thin perovskite matrix less than a few nanometers thick. While this method resulted in the formation of bulk perovskite on the CQD film, the overgrown perovskite layer formed on the surface could be easily removed by washing with ACN solvent. In the grazing-incidence small-angle x-ray scattering (GISAX) analysis, even after the ACN washing step, the decreased dot-to-dot distance in the CQD film resulting from the formation of the dot-in-perovskite matrix did not revert to its initial state. The HR-TEM images of the dot-in-perovskite film before and after ACN washing both showed epitaxial coupling between PbS (111)-$FAPbBr_3$ (100)-PbS (111) [Fig. 3(b)]. However, the bare CQD film exhibited randomly oriented coupling. Additionally, before the ACN washing step, the two-photon ultrafast transient absorption (2PTA) spectrum of the dot-in-perovskite CQD film revealed signals around 750 and 550 nm, corresponding to bulk and 2D perovskite, respectively. However, after ACN washing, only the signal for 2D perovskite was detected. These results demonstrate that the washing step only eliminates the top-area perovskite crystals without affecting the overall matrix structure. After two years, in 2022, Ding *et al.* reported achieving a PCE of 15.5% by engineering the interfaces of $FAPbX_3$ (X = I, Br) based dot-in-perovskite CQD photovoltaics (The PCE of control device, without interface engineering is 13.1%).[38] They achieved this by introducing a mixture of polymethyl methacrylate (PMMA) and [6,6]-phenyl-C61-butyric acid methyl ester (PCBM), as well as a PMMA-graphene oxide (GO) interlayer, between the interfaces of the electron transport layer (ETL)/CQD and CQD/hole transport layer (HTL) [Fig. 3(c)].

D. Quantum dot-in-perovskite for other electronics

The advantages of dot-in-perovskite hybrids can extend beyond photovoltaics. In 2016, Gong *et al.* reported significant advancements in near-infrared (NIR) CQD light emitting diodes (LEDs) by incorporating the PbS-$MAPbI_3$ dot-in-perovskite structure.[30] Compared to bare CQD NIR LEDs, those with dot-in-perovskite demonstrated a remarkable 3.5 times enhancement in electroluminescence (EL) efficiency. Particularly noteworthy in this study is the investigation into the effects of adding bromide to the $MAPbI_3$ perovskite matrix. This strategy led to an overall improvement in the performance of the NIR LED device, attributed to the reduced lattice mismatch between the perovskite–CQD interface. However, the optimal lattice matching condition did not directly correlate with the best device performance. While the lowest lattice mismatch was achieved at a composition ratio of Br:I to 1:2, the carrier diffusion length [Fig. 3(a)] and PLQE [Fig. 3(b)] were highest at iodide concentrations of 83% and 50%, respectively. Although the origin of these results was not identified, we can hypothesize that it is due to the trade-off relationship between "increasing the energy barrier of the type-I electronic structure between the CQD-perovskite matrix via bromide addition" and "decreasing surface defects by increasing lattice matching."

Dot-in-perovskite hybridization has also been employed to CQD photodetectors. In a 2017 study, Sytnyk *et al.* reported a dot-in-perovskite structured CQD photodetector with a detectivity of 2×10^{11} cm $Hz^{1/2}/W$ (Jones), using MA bismuth iodide perovskite (MA_3BiI_6).[32] The similar anion-cation bond length between the PbS crystal and Bi I_6^{3-} enables the epitaxial growth of MA_3BiI_6. Additionally, they noted the faster reactivity and higher dispersion stability of the hexahalide perovskite precursor compared to the trihalide perovskite precursor. Notably, the MA_3BiI_6 perovskite and PbS CQD exhibit a type-II band alignment, which is a staggered electronic structure that promotes the effective separation of electrons and holes, resulting in reduced carrier recombination and enhanced photoconductivity [Fig. 4(c)]. In 2023, Chen *et al.* improved the EQE and detectivity of NIR-CQD photodetectors from 35% and 1.7×10^{12} to 52% and 6.2×10^{12} Jones, respectively, through dot-in-perovskite hybridization using the $CsPbX_3$ (X = Br, I) perovskite matrix.[39] The DFT results of this study revealed that the epitaxial growth of $CsPbBr_3$ is more favorable on PbS (100) facets than on (111) facets due to the lower interfacial energy of on $CsPbBr_3$-PbS (100) compared to $CsPbBr_3$-PbS (100) (each 3.9 and 6.9 eV), suggesting that Cs cation-based perovskites are suitable for hybridization with large-sized PbS CQDs over ~4 nm [Fig. 4(d)].

III. CONCLUSIONS AND FUTURE PERSPECTIVES OF QUANTUM DOT-IN-PEROVSKITE HYBRIDS

We chronicled the history of dot-in-perovskite hybridization between PbS CQDs and lead halide perovskites. Although this hybrid was initially aimed at combining the strengths of two materials (the tunable absorption range with IR capability of CQDs and the long-range carrier transport of perovskites),[27] subsequent studies revealed additional benefits of dot-in-perovskite hybridization of CQDs and perovskites (Table I).[28–41] From our perspective, the most notable improvement is the enhanced thermal stability of CQD films through

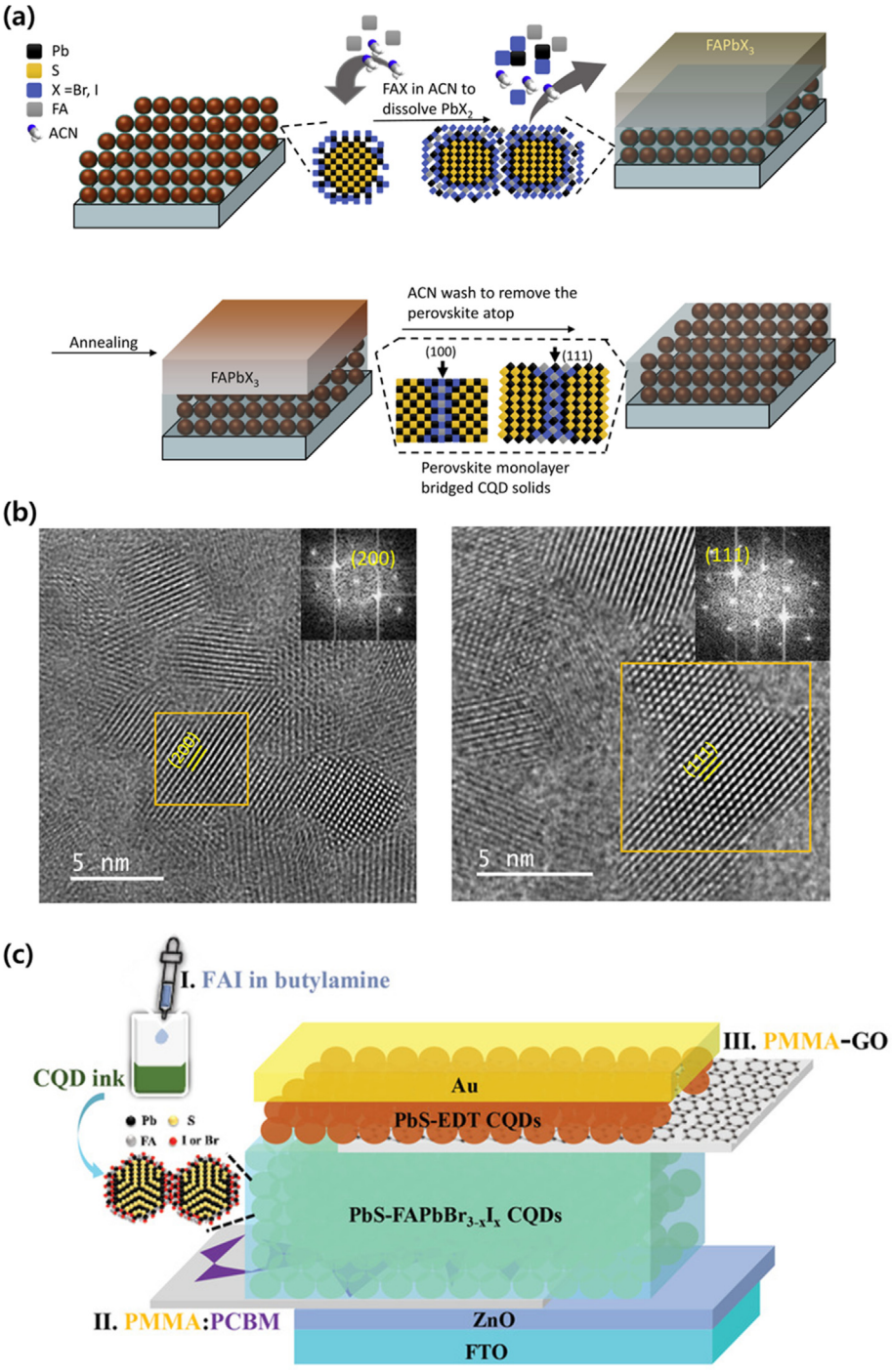

FIG. 3. (a) Schematic of the fabrication process for monolayer perovskite bridges: The perovskite matrix is formed by soaking a CQD-PbX_2 film in an FAX (X = Br, I) solution. Here, the FAX solution dissolves PbX_2 ligands and promotes the growth of perovskite between neighboring PbS CQDs. The CQD films are annealed and then washed with acetonitrile (ACN) to remove excess material. Reproduced with permission from Joule **4**, 1542–1556 (2020). Copyright 2020 Cell Press.[37] (b) High-resolution transmission electron microscopy (HRTEM) image of a CQD cluster connected along the (200) facet (left) and the (111) facet (right). Reproduced with permission from Joule **4**, 1542–1556 (2020). Copyright 2020 Cell Press.[37] The insets display the selected-area electron diffraction patterns for each facet. (c) Schematic illustration of interface-engineered PbS-$FAPbX_3$ dot-in-perovskite CQD photovoltaic. Reproduced with permission from Adv. Energy Mater. **12**, 2201676 (2022). Copyright 2022 Wiley-VCH.[38]

these hybridizations.[34] Unlike conventional surface passivation methods, which are vulnerable to ligand losses and oxidation, the dot-in-perovskite structure physically protects the CQDs from degradation. Therefore, it is anticipated that the emerging CQD-perovskite hybridization strategy could be a breakthrough technology for addressing the thermal stability issues of CQDs observed in past decades. However, studies on CQD photovoltaics that adopted the dot-in-perovskite structure did not report enhanced thermal stability. This absence could be addressed by developing thermally stable charge transport materials for CQD photovoltaics.

Additionally, to fabricate CQD photovoltaics with a dot-in-perovskite structure that exhibits excellent thermal stability, it is

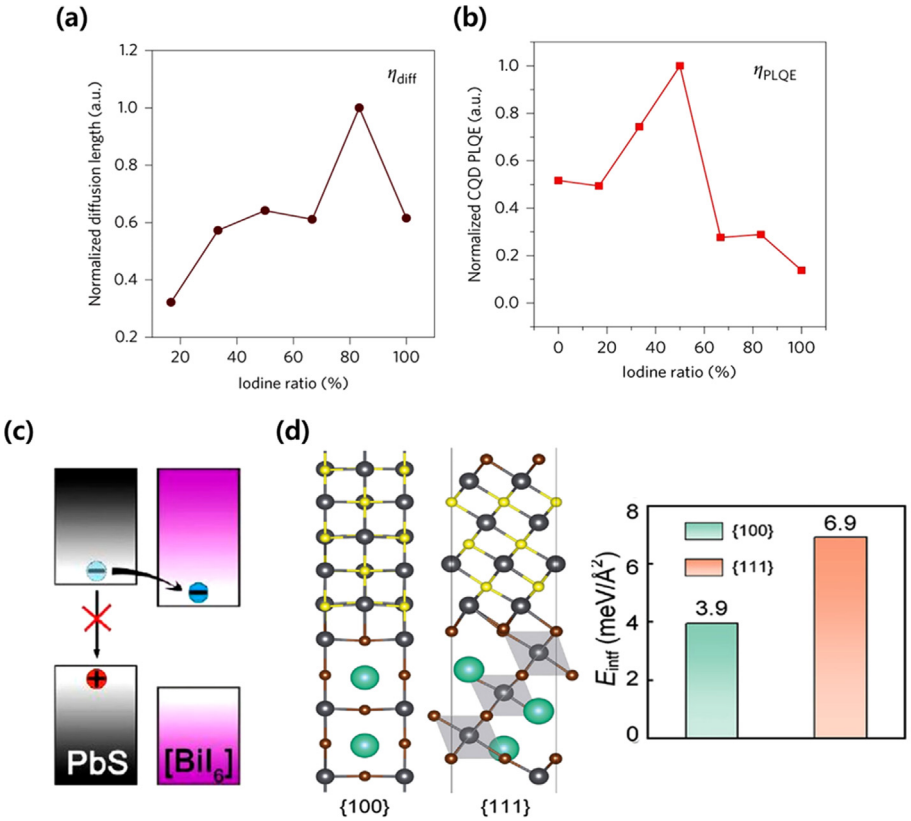

FIG. 4. (a) Normalized diffusion length and (b) PLQE of PbS CQDs embedded in a $MAPbX_3$ (X = Br, I) perovskite matrix with various iodine concentrations. Reproduced with permission from Nat. Photon. **10**, 253–257 (2016). Copyright 2016 Springer Nature.[30] (c) Type-II band alignment between PbS CQD and MA_3BiI_6 perovskite. Reproduced with permission from ACS Nano. **11**, 1246–1256 (2017). Copyright 2017 America Chemical Society.[32] (d) The interface model and interfacial energy of $CsPbBr_3$-PbS (100) (left) and $CsPbBr_3$-PbS (111) (right); the black, yellow, green, and brown spheres in the schematic represent Pb, S, Cs, and Br, respectively. Reproduced with permission from Adv. Funct. Mater. **33**, 2210158 (2023). Copyright 2023 Wiley-VCH.[39]

TABLE I. Device parameters and stability of dot-in-perovskite-based photovoltaics.

Device structure	V_{OC} (V)	J_{SC} (mA/cm^2)	FF (%)	PCE (%)	Stability test	Year	Ref
ITO/ZnO/PbS-$MAPbI_3$/PbS-EDT/Au	0.61	21.9	68	8.95	–	2015	28
ITO/MZO/PbS-$CsPbI_3$/PbS-EDT/Au	0.64	24.5	67	10.5	After 46 hours aging, 88% of the initial efficiency is maintained.	2018	33
ITO/ZnO/PbS-$CsPbX_3$/PbS-EDT/Au	0.64	28.9	68.4	12.6	After 2 hours of continuous AM1.5G illumination in an unencapsulated state, retains 95% of the initial PCE.	2020	34
ITO/ZnO/PbS-CSMAFA/PbS-EDT/Au	0.59	27.4	65.6	10.6	The CsMAFA devices retain 96% of their performance after about 1200h ambient storage.	2020	36
ITO/ZnO/PbS-$FAPbBr_3$/PbS-EDT/Au	0.65	30	71	13.8	After continuous AM1.5G illumination for 2.8 hours in N_2, it decreased to 60% of initial PCE after 380 hours.	2020	37
FTO/ZnO/PbS-$FAPbBr_2I$/PbS-EDT/Au	0.66	31.5	74.3	15.5	Retain over 90% of its highest average PCE after 160 days dry air storage	2022	38
FTO/TiO_2/$MAPbI_3$-PbS/spiro-OMeTAD/Au	1.028	23.5	77.2	18.6	–	2018	40
FTO/TiO_2/$MAPbI_3$-PbS doping/Spiro-MeTAD/Au	1.07	21.1	77	17.4	–	2018	29
FTO/SnO_2/$FAPbI_3$-PbS/spiro-OMeTAD/Au	1.105	21.5	75.7	18	After 720 h, it retains 86% of initial PCE	2020	41

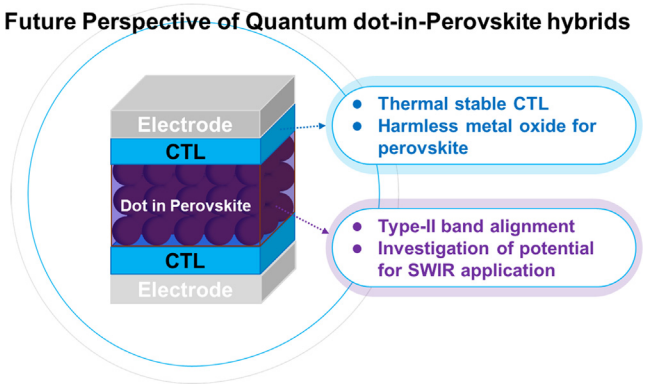

FIG. 5. Suggested four perspectives of future research direction of dot-in-perovskite hybrids for optoelectronics.

essential to select charge transport materials that do not induce adverse chemical decomposition in the perovskite layer. For instance, zinc oxide (ZnO) and MA-based lead halide perovskites are not chemically compatible; the basic nature of ZnO leads to the deprotonation of methylammonium cations in the adjacent perovskite layer, resulting in the formation of methylamine and PbI_2 during thermal exposure. Therefore, it is crucial to carefully choose combinations that do not compromise the thermal stability and electrical properties of the perovskite due to the charge transport material. The effective operation of dot-in-perovskite CQD photovoltaics reported so far, despite the use of ZnO as an ETL, may stem from the stabilization of the perovskite crystal due to a lattice anchoring effect. Nevertheless, given the chemical sensitivity of perovskite, there remains room for further improvement in dot-in-perovskite-based devices through careful selection of the electron transport material. Meanwhile, factors like lattice matching and interfacial energy are critical in the formation of dot-in-perovskite structures. As such, research to date has primarily concentrated on these interfacial conditions, particularly on customizing the composition of perovskites by adjusting organic/inorganic cations and halide anions. Referring to the traditional III-V CQD and core-shell II-VI communities, we can conclude that future studies need to thoroughly explore the energy band structure between the CQDs and perovskites to enhance charge extraction in dot-in-perovskite films.[56–60] These studies indicate that type-I electronic structures are not ideal for charge extraction, as they confine the electron and hole wave functions to a narrower bandgap region, creating an energy barrier that hampers charge extraction. However, most reported dot-in-perovskite hybrids exhibit type-I band alignment, characterized by a sandwiched band structure between the perovskite matrix and the embedded CQDs. This alignment occurs because perovskites typically have larger band gaps compared to CQDs. Therefore, to achieve more efficient charge separation, future research should aim to develop type-II band alignment, which features a staggered bandgap between CQDs and perovskites, in upcoming composition engineering efforts.

Additionally, we hope that the dot-in-perovskite hybrids using SWIR harvesting CQDs will be intensively studied. To fully capitalize on the large absorption range potential of PbS CQDs, it is essential to use large-sized CQDs over ~4 nm.[15,61–63] However, conventional surface passivation strategies for PbS CQDs are primarily developed for smaller-sized CQDs under ~3 nm. This is due to the relative difficulty of ligand binding on the non-polar (100) facet, which is predominant in large-sized CQDs.[19,62] On the other hand, DFT results from recent dot-in-perovskite studies have revealed that the epitaxial growth of lead halide perovskite is more favorable on the PbS (100) facet than on the PbS (111) facet, suggesting significant potential for dot-in-perovskite hybridizations in SWIR devices or tandem photovoltaics (Fig. 5).

ACKNOWLEDGMENTS

This research was supported by the Nano & Material Technology Development Program through the National Research Foundation of Korea (NRF), funded by Ministry of Science and ICT (Grant No. RS-2024-00451318), and the Basic Research Lab (Grant No. RS-2023-00223196) through the National Research Foundation (NRF) of Korea.

AUTHOR DECLARATIONS

Conflict of Interest

The authors have no conflicts to disclose.

Author Contributions

Hyung Ryul You: Data curation (equal); Writing – original draft (equal); Writing – review & editing (equal). **Han Na Yu:** Data curation (equal); Writing – original draft (equal); Writing – review & editing (equal). **Eon Ji Lee:** Writing – review & editing (equal). **Hyeon Soo Ma:** Writing – review & editing (equal). **Younghoon Kim:** Data curation (equal); Writing – original draft (equal); Writing – review & editing (equal). **Jongmin Choi:** Supervision (equal); Writing – original draft (equal).

DATA AVAILABILITY

The data that support the findings of this study are available from the corresponding author upon reasonable request.

REFERENCES

[1]W. Shockley and H. J. Queisser, J. Appl. Phys. **32**, 510–519 (1961).
[2]A. De Vos and H. Pauwels, Appl. Phys. **25**, 119–125 (1981).
[3]E. Semonin, J. M. Luther, and M. C. Beard, Mater. Today **15**, 508 (2012).
[4]G. Konstantatos, I. Howard, A. Fischer, S. Hoogland, J. Clifford, E. Klem, L. Levina, and E. H. Sargent, Nature **442**, 180 (2006).
[5]R. D. Schaller and V. I. Klimov, Phys. Rev. Lett. **92**, 186601 (2004).
[6]M. C. Beard, K. P. Knutsen, P. Yu, J. M. Luther, Q. Song, W. K. Metzger, R. J. Ellingson, and A. J. Nozik, Nano Lett. **7**, 2506–2512 (2007).
[7]D. J. Norris and M. G. Bawendi, Phys. Rev. B. **53**, 16338–16346 (1996).
[8]S. W. Baek, J. H. Song, W. Choi, H. Song, S. Jeong, and J. Y. Lee, Adv. Mater. **27**, 8102 (2015).
[9]D. Zhao, J. Huang, R. Qin, G. Yang, and J. Yu, Adv. Opt. Mater. **6**, 1800979 (2018).
[10]J. Kim, S. Han, G. Lee, J. Choi, M. Ko, and Y. Kim, Chem. Eng. J. **448**, 137672 (2022).
[11]L. Duan, L. Hu, X. Guan, C.-H. Lin, D. Chu, S. Huang, X. Liu, J. Yuan, and T. Wu, Adv. Energy Mater. **11**, 2100354 (2021).
[12]M. Yuan, M. Liu, and E. H. Sargent, Nat. Energy **1**, 16016 (2016).
[13]Y. Kim, M.-J. Choi, and J. Choi, J. Mater. Sci. Technol. **147**, 224–240 (2023).
[14]P. R. Brown, D. Kim, R. R. Lunt, N. Zhao, M. G. Bawendi, J. C. Grossman, and V. Bulovic, ACS Nano **8**, 5863–5872 (2014).
[15]M. A. Hines and G. D. Scholes, Adv. Mater. **15**, 1844–1849 (2003).

[16]Z. Ning, O. Voznyy, J. Pan, S. Hoogland, V. Adinolfi, J. Xu, M. Li, A. R. Kirmani, J. P. Sun, J. Minor, K. W. Kemp, H. Dong, L. Rollny, A. Labelle, G. Carey, B. Sutherland, I. Hill, A. Amassian, H. Liu, J. Tang, O. M. Bakr, and E. H. Sargent, Nat. Mater. **13**, 822 (2014).
[17]C. H. Chung, P. R. Brown, V. Bulovic, and M. G. Bawendi, Nat. Mater. **13**, 796 (2014).
[18]M. Liu, O. Voznyy, R. Sabatini, F. P. G. de Arquer, R. Munir, A. H. Balawi, X. Lan, F. Fan, G. Walters, A. R. Kirmani, S. Hoogland, F. Laquai, A. Amassian, and E. H. Sargent, Nat. Mater **16**, 258 (2017).
[19]Y. Kim, F. Che, J. W. Jo, J. Choi, F. P. Garcia de Arquer, O. Voznyy, B. Sun, J. Kim, M. J. Choi, R. Quintero-Bermudez, F. Fan, C. S. Tan, E. Bladt, G. Walters, A. H. Proppe, C. Zou, H. Yuan, S. Bals, J. Hofkens, M. B. J. Roeffaers, S. Hoogland, and E. H. Sargent, Adv. Mater. **31**, 1805580 (2019).
[20]M. J. Choi, F. P. Garcia de Arquer, A. H. Proppe, A. Seifitokaldani, J. Choi, J. Kim, S. W. Baek, M. Liu, B. Sun, M. Biondi, B. Scheffel, G. Walters, D. H. Nam, J. W. Jo, O. Ouellette, O. Voznyy, S. Hoogland, S. O. Kelley, Y. S. Jung, and E. H. Sargent, Nat. Commun. **11**, 103 (2020).
[21]J. Choi, M. J. Choi, J. Kim, F. Dinic, P. Todorovic, B. Sun, M. Wei, S. W. Baek, S. Hoogland, F. P. G. de Arquer, O. Voznyy, and E. H. Sargent, Adv. Mater. **32**, 1906497 (2020).
[22]B. Kim, S. W. Baek, C. Kim, J. Kim, and J. Y. Lee, Adv. Energy Mater. **12**, 2102689 (2022).
[23]H. R. You, S. Lee, D. H. Lee, G. Murali, A. S. Nissimagoudar, Y. Kim, S. Park, J. Lee, S. J. Kim, J. Y. Park, B. J. Moon, Y. H. Park, S.-K. Kim, H. N. Yu, H. J. Kim, W. Lee, G. Ham, H. Lee, S.-C. Lee, H. Cha, J. Lim, Y. Gogotsi, T. K. An, I. In, and J. Choi, Adv. Energy Mater. **13**, 2301648 (2023).
[24]C. Wang, Q. Wu, Y. Wang, Z. Wang, H. Li, X. Li, X. Chen, C. Wang, Y. Liu, and X. Zhang, Adv. Funct. Mater. **34**, 2315365 (2024).
[25]E. J. Lee, W. Lee, T. H. Yun, H. R. You, H. J. Kim, H. N. Yu, S.-K. Kim, Y. Kim, H. Ahn, J. Lim, C. Yim, and J. Choi, Small **20**, 2400380 (2024).
[26]J. Liu, K. Xian, L. Ye, and Z. Zhou, Adv. Mater. **33**, 2008115 (2021).
[27]Z. Ning, X. Gong, R. Comin, G. Walters, F. Fan, O. Voznyy, E. Yassitepe, A. Buin, S. Hoogland, and E. H. Sargent, Nature **523**, 324–328 (2015).
[28]Z. Yang, A. Janmohamed, X. Lan, F. P. G. de Arquer, O. Voznyy, E. Yassitepe, G.-H. Kim, Z. Ning, X. Gong, R. Comin, and E. H. Sargent, Nano Lett. **15**, 7539–7543 (2015).
[29]S.-S. Li, C.-H. Chang, Y.-C. Wang, C.-W. Lin, D.-Y. Wang, J.-C. Lin, C.-C. Chen, H.-S. Sheu, H.-C. Chia, W.-R. Wu, U.-S. Jeng, C.-T. Liang, R. Sankar, F.-C. Chou, and C.-W. Chen, Energy Environ. Sci. **9**, 1282–1289 (2016).
[30]X. Gong, Z. Yang, G. Walters, R. Comin, Z. Ning, E. Beauregard, V. Adinolfi, O. Voznyy, and E. H. Sargent, Nat. Photon. **10**, 253–257 (2016).
[31]Y.-K. Jung, K. T. Butler, and A. Walsh, J. Phys. Chem. C. **121**, 27351–27356 (2017).
[32]M. Sytnyk, S. Yakunin, W. Schöfberger, R. T. Lechner, M. Burian, L. Ludescher, N. A. Killilea, A. YousefiAmin, D. Kriegner, J. Stangl, H. Groiss, and W. Heiss, ACS Nano. **11**, 1246–1256 (2017).
[33]X. Zhang, J. Zhang, D. Phuyal, J. Du, L. Tian, V. A. Öberg, M. B. Johansson, U. B. Cappel, O. Karis, J. Liu, H. Rensmo, G. Boschloo, and E. M. J. Johansson, Adv. Energy Mater. **8**, 1702049 (2018).
[34]M. Liu, Y. Chen, C.-S. Tan, R. Quintero-Bermudez, A. H. Proppe, R. Munir, H. Tan, O. Voznyy, B. Scheffel, G. Walters, A. P. T. Kam, B. Sun, M.-J. Choi, S. Hoogland, A. Amassian, S. O. Kelley, F. P. García de Arquer, and E. H. Sargent, Nature **570**, 96–100 (2019).
[35]E. A. Gaulding, X. Chen, Y. Yang, S. P. Harvey, B. To, Y.-H. Kim, M. C. Beard, P. C. Sercel, and J. M. Luther, ACS Mater. Lett. **2**, 1464–1472 (2020).
[36]M. Albaladejo-Siguan, D. Becker-Koch, A. D. Taylor, Q. Sun, V. Lami, P. G. Oppenheimer, F. Paulus, and Y. Vaynzof, ACS Nano. **14**, 384–393 (2020).
[37]B. Sun, A. Johnston, C. Xu, M. Wei, Z. Huang, Z. Jiang, H. Zhou, Y. Gao, Y. Dong, O. Ouellette, X. Zheng, J. Liu, M.-J. Choi, Y. Gao, S. W. Baek, F. Laquai, O. M. Bakr, D. Ban, O. Voznyy, F. P. García de Arquer, and E. H. Sargent, Joule. **4**, 1542–1556 (2020).
[38]C. Ding, D. Wang, D. Liu, H. Li, Y. Li, S. Hayase, T. Sogabe, T. Masuda, Y. Zhou, Y. Yao, Z. Zou, R. Wang, and Q. Shen, Adv. Energy Mater. **12**, 2201676 (2022).
[39]D. Chen, Y. Liu, B. Xia, L. Chen, Y. Yang, G. Yang, J. Liu, S. Lu, C. Ge, P. Liu, J. Yang, G. Liang, X. Lan, X. Zeng, L. Li, J. Zhang, Z. Xiao, L. Gao, and J. Tang, Adv. Funct. Mater. **33**, 2210158 (2023).
[40]J. Han, S. Luo, X. Yin, Y. Zhou, H. Nan, J. Li, X. Li, D. Oron, H. Shen, and H. Lin, Small. **14**, 1801016 (2018).
[41]S. Masi, C. Echeverría-Arrondo, K. M. M. Salim, T. T. Ngo, P. F. Mendez, E. López-Fraguas, D. F. Macias-Pinilla, J. Planelles, J. I. Climente, and I. Mora-Sero, ACS Energy Lett. **5**, 418–427 (2020).
[42]S. Sun, T. Salim, N. Mathews, M. Duchamp, C. Boothroyd, G. Xing, T. C. Sum, and Y. M. Lam, Energy Environ. Sci. **7**, 399–407 (2014).
[43]A. Kojima, K. Teshima, Y. Shirai, and T. Miyasaka, J. Am. Chem. Soc. **131**, 6050–6051 (2009).
[44]H. Min, D. Y. Lee, J. Kim, G. Kim, K. S. Lee, J. Kim, M. J. Paik, Y. K. Kim, K. S. Kim, M. G. Kim, T. J. Shin, and S. I. Seok, Nature. **598**, 444–446 (2021).
[45]J. Park, J. Kim, H.-S. Yun, M. J. Paik, E. Noh, H. J. Mun, M. G. Kim, T. J. Shin, and S. I. Seok, Nature. **616**, 724–727 (2023).
[46]H. Min, M. Kim, S.-U. Lee, H. Kim, G. Kim, K. Choi, J. H. Lee, and S. I. Seok, Science. **366**, 749–753 (2019).
[47]N. J. Jeon, J. H. Noh, W. S. Yang, Y. C. Kim, S. Ryu, J. Seo, and S. I. Seok, Nature. **517**, 476–480 (2015).
[48]M. V. Dambhare, A. Ugale, B. P. Butey, S. P. Wankhede, and S. V. Moharil, AIP Conf. Proc. **2974**, 020036 (2024).
[49]Q. Wang, X. Zheng, Y. Deng, J. Zhao, Z. Chen, and J. Huang, Joule. **1**, 371–382 (2017).
[50]G. E. Eperon and D. S. Ginger, ACS Energy Lett. **2**, 1190–1196 (2017).
[51]R. C. Keitel, M. C. Weidman, and W. A. Tisdale, J. Phys. Chem. C. **120**, 20341–20349 (2016).
[52]R. Ihly, J. Tolentino, Y. Liu, M. Gibbs, and M. Law, ACS Nano **5**, 8175–8186 (2011).
[53]M. Li, R. Sun, J. Chang, J. Dong, Q. Tian, H. Wang, Z. Li, P. Yang, H. Shi, C. Yang, Z. Wu, R. Li, Y. Yang, A. Wang, S. Zhang, F. Wang, W. Huang, and T. Qin, Nat. Commun. **14**, 573 (2023).
[54]A. Amat, E. Mosconi, E. Ronca, C. Quarti, P. Umari, M. K. Nazeeruddin, M. Gratzel, and F. D. Angelis, Nano Lett. **14**, 3608–3616 (2014).
[55]K. Schutt, P. K. Nayak, A. J. Ramadan, B. Wenger, Y.-H. Lin, and H. J. Snaith, Adv. Funct. Mater. **29**, 1900466 (2019).
[56]P. Reiss, M. Protiere, and L. Li, Small **5**, 154–168 (2009).
[57]G. S. Selopal, H. Zhao, Z. M. Wang, and F. Rosei, Adv. Funct. Mater. **30**, 1908762 (2020).
[58]P. Maity, T. Debnath, and H. N. Ghosh, J. Phys. Chem. C **119**, 26202 (2015).
[59]R. B. Laghumavarapu, A. Moscho, A. Khoshakhlagh, M. EI-Emawy, L. F. Lester, and D. L. Huffaker, Appl. Phys. Lett. **90**, 173125 (2007).
[60]E. Antolin, A. Marti, C. D. Farmer, P. G. Linares, E. Hernandez, A. M. Sanchez, T. Ben, S. I. Molina, C. R. Stanley, and A. Luque, J. Appl. Phys **108**, 64513 (2010).
[61]J. Wang, I. Mora-Sero, Z. X. Pan, K. Zhao, H. Zhang, Y. Y. Feng, G. Yang, X. H. Zhong, and J. Bisquert, J. Am. Chem. Soc. **135**, 15913 (2013).
[62]M. Li, J. Yan, X. Zhao, T. Ma, A. Zhang, S. Chen, G. Shen, G. Mohamed, G. Khalaf, J. Zhang, C. Chen, H.-Y. Hsu, H. Song, P. Yang, and J. Tang, Adv. Energy Mater. **14**, 2400219 (2024).
[63]I. Moreels, K. Lambert, D. Smeets, D. D. Muynck, T. Nollet, J. C. Martins, F. Vanhaecke, A. Vantomme, C. Delerue, G. Allan, and Z. Hens, ACS Nano **3**, 3023–3030 (2009).